vQRS Based on Hybrids of CNT with PMMA-POSS and PS-POSS Copolymers to Reach the Sub-PPM Detection of Ammonia and Formaldehyde at Room Temperature Despite Moisture

Abhishek Sachan [1,2], Mickael Castro [1], Veena Choudhary [2] and Jean-François Feller [1,*]

[1] Smart Plastics Group, Bretagne Loire University (UBL), IRDL CNRS 3744-UBS, Lorient 56321, France; abhishek.sachan@univ-ubs.fr (A.S.); mickael.castro@univ-ubs.fr (M.C.)

[2] Indian Institute of Technology (IIT), Centre for Polymer Science & Engineering, Delhi 110016, India; veenac@polymers.iitd.ac.in

* Correspondence: jean-francois.feller@univ-ubs.fr

Abstract: Nanocomposite-based quantum resistive vapour sensors (vQRS) have been developed from the assembly of hybrid copolymers of polyhedral oligomeric silsesquioxane (POSS) and poly(methyl methacrylate) (PMMA) or poly(styrene) (PS) with carbon nanotubes (CNT). The originality of the resulting conducting architecture is expected to be responsible for the ability of the transducer to detect sub-ppm concentrations of ammonia and formaldehyde at room temperature despite the presence of humidity. In particular, the boosting effect of POSS is evidenced in CNT-based nanocomposite vQRS. The additive fabrication by spraying layer-by-layer provides (sLbL) is an effective method to control the reproducibility of the transducers' chemo-resistive responses. In dry atmosphere, the two types of sensors showed a high sensitivity towards both hazardous gases, as they were able to detect 300 ppb of formaldehyde and 500 ppb of ammonia with a sufficiently good signal to noise ratio (SNR > 10). They also exhibited a quick response times less than 5 s for both vapours and, even in the presence of 100 ppm of water, they were able to detect small amounts of gases (1.5 ppm of NH_3 and 9 ppm of CH_2O). The results suggest promising applications of POSS-based vQRS for air quality or volatolome monitoring.

Keywords: quantum resistive vapour sensor; toxic gases sub ppm detection; ammonia; formaldehyde; room-temperature; nanocomposite; humidity; spraying layer-by-layer

1. Introduction

There are now much evidence that environmental issues are related to human activity growth, in particular global warming, and water and air pollution. The latter results in serious troubles to human health, as frequently pointed out by the World Health Organization (WHO) [1]. The WHO reported that 8.2 million deaths caused by the environment come from non-communicable diseases, such as stroke, heart disease, cancers, and chronic respiratory disease, which now amounts to nearly two-thirds of the total deaths caused by unhealthy environments [2]. Figure 1 shows the death attributable to joint effects of both household and ambient air pollution. Actually, one-third of cancer deaths could be prevented by anticipated diagnosis and this perspective holds significant potential to solve this issue [3,4].
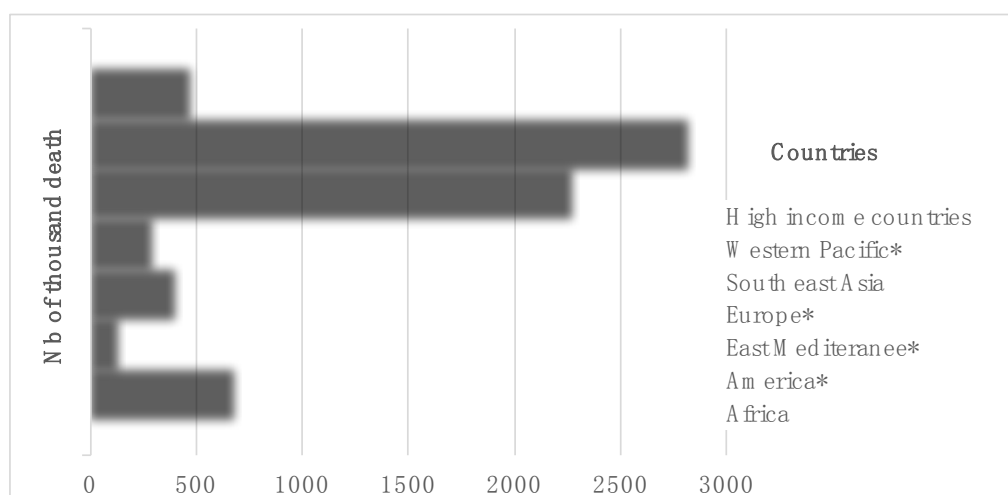
Figure 1. According to the world health organization (WHO), air pollution is now one of the world's largest health risks when excluding communicable diseases; deaths attributable to joint effects of both household and ambient air pollution [5]. * Low and middle income countries.

Therefore, different strategies can be envisaged to counterbalance this trend and enhance people's quality of life. Trying to reduce the impacts of human activity on the environment seems a difficult and long-term task, although necessary to lead. However, developing anticipation tools for the early diagnosis of cancer or monitoring air quality, and, in particular toxic vapours, must be more effective in the short-term. In this context the detection of toxic gases, such as ammonia (NH_3), is of great interest especially for environmental gas monitoring [6], exhaust gas determination in automobiles [7], leakage detection in chemical plants [8], and product quality assurance in food companies [9]. The limit of concentration of short term exposure to ammonia is 50 ppm for 30 min [10], while for longer times it is only 20 ppm. Classical ammonia sensors are mainly based on metal oxides (MOx) [11], intrinsically-conducting polymers (ICP) [12], catalytic sensors [13], and spectrophotometric detection [14]. Nevertheless, the detection of ammonia at the sub-ppm level remains challenging for most of these sensors, which require high temperatures to activate, react with ammonia molecules, or eliminate moisture [15,16]. Additionally, ICP-based sensors can lack reproducibility due to the dependency of their responses' amplitude on several parameters, such as the active layer thickness and morphology, its porosity, the nature of the dopant, and the presence of other components in the material [12]. Several works also mention the use of carbon nanotube-based sensors for the detection of ammonia [17–19], but CNTs without functionalization have poor chemical selectivity [20] and the resulting conducting architecture tends to have a poor structural stability when assembled without any binder or matrix [21]. This is why several researchers have experimented the functionalization of CNT by insulating polymers, like PMMA [22] chitosan [23], poly(lactic acid) PLA [24], or intrinsically-conducting polymers (ICP), like poly(pyrrole) (PPy) [25–27], poly(thiophene) (PEDOT) [27,28], or poly(aniline) (PANI) [27,28], which can lead to a positive synergy. However, it seems that reaching the ppb range of detection makes the use of nanostructured transducers compulsory, as only the few works using this strategy report such a high sensitivity. Wojkiewicz et al. [12] synthesized three kinds of nanostructured thin transducing films, from the assembly of poly(butadiene) (PBuA–PANI), poly(vinyl fluoride) (PVDF-PANI) core/shell nanoparticles, and PANI (CSA) nanofibers filled poly(urethane) films, demonstrating their ability to detect, respectively, 250, 100, and 20 ppb of NH_3. Moreover, the chemo-resistive signals of these systems are found to be reproducible and with low noise, but their recovery time is long (more than 20 min), compared to the exposure time of analytes of 5 min.

Table 1 summarises the performances of some chemo-resistive nanocomposite transducers for ammonia sensing found in the literature compared to the transducer developed in the present study.

Table 1. Ammonia sensing performances of some nanocomposite sensors, Op.: Operating.

Transducer	LOD	Mechanism	Op. Temp °C	Reference
PMMA-POSS/CNT	0.5 ppm	Chemo-resistive	25	This work
V_2O_5 and V_7O_{16} film	0.2 ppm	Chemo-resistive	350	[29]
SnO_2-Nb-Pt nanocrystaline	10 ppm	Chemo-resistive	355	[30]
Nanoporous NiO film	20 ppm	Chemo-resistive	250	[31]
PPy NP	5 ppm	Chemo-resistive	25	[32]
TiO_2 NP deco GR/PPy	1 ppm	Chemo-resistive	25	[33]

Formaldehyde (CH_2O) is another common toxic gas that can be found inside buildings [34]. Mostly household, wooden, and plastic products or carpeting emit formaldehyde [35–37]. The limit concentration of short-term exposure to formaldehyde is 0.08 ppm for 30 min [38] and 0.016 ppm for long-term exposure [39]. Different types of sensors have been developed in the literature to detect formaldehyde, such as spectro-colorimetric sensors by Suzuki et al., who made a device using organic molecules that change colour when reacting with CH_2O [40], or amperometric sensors which take benefit from an enzymatic reaction with formaldehyde molecules, which changes the electrical current in the transducer [41]. Other sensors use metal oxides or have very complex testing setups and generally require high working temperatures, for instance, SiO_2-NiO-based formaldehyde sensors that operate at 300 °C [42]. Li et al. [43] have tested Au-In_2O_3 and In_2O_3 nanoparticle-based sensors for the detection of ammonia and formaldehyde at the concentration of 100 ppm. Nevertheless, metal oxide-based gas sensors still require high operating temperatures (ca. 300–400 °C) to allow signal recovery after analyte exposure and to eliminate undesirable resistance variations, which is energy consuming, and does not seem to completely fix baselines drifting upon oxidation by the tested gases [44]. Nevertheless, some MOx hybrids were found to operate at room temperature with ppm sensitivity [45,46]. Additionally, some strategies have been developed to increase their limit of detection at the ppb level by decreasing the size of active particles (resulting in an increase of porosity). For instance, hierarchically porous indium oxide In_2O_3 nanolamellae with two levels of nanopores were found able to detect 80 ppb of CH_2O although with a rather low signal-to-noise ratio [47], and CuO_2 nanocubes could reach the very low limit of detection of 6 ppb of CH_2O [48]. To take benefit from nanostructuring and overcome the low selectivity of metal oxide transducers, Güntner et al. [49] used flame spray pyrolysis to develop aggregates of SnO_2 nanoparticles doped with Pt, Si, Ti, and Pd to selectively detect analytes, such as CH_2O (at 30 ppb) and NH_3 (at 250 ppb), in the presence of 90% H_2O. The fact that SnO_2 sensors were able to operate in such difficult conditions is encouraging for breath analysis, but they maintain a strong temperature dependency requiring reaching 400 °C to stabilize the resistance and allow the full signal recovery, consuming about 500 mW per sensor.

From this non-exhaustive overview on the different strategies used to sense CH_2O and NH_3 at the very low concentration at which they are toxic, i.e., the sub-ppm level, the best results were obtained with MOx- [49] or ICP-based [12] nanostructured resistive sensors. However, it can also be concluded that there is still a challenge to develop vapour sensors: highly-sensitive and -selective to CH_2O and NH_3, operating at room temperature to minimize consumption, working in high moisture environments, and easily up-scalable into e-nose applications. In this context, we have used our experience in the design of quantum resistive vapour sensors (vQRS) that already proved their sub-ppm sensitivity to VOCs [50] and robustness towards 50% moisture [51] to investigate their performances in this new frame and, accordingly, develop new sensors eventually integrable in an e-nose. Carbon nanotubes were chosen to build the sensors' conducting architecture because of their exceptional aspect ratio, electrical conductivity, and ability to form light and easily-switchable interconnected networks [52]. Polyhedral oligomeric silsesquioxane (POSS) was selected in this study because it recently proved to be an effective nanobrick to provide a nano-assembled conducting architecture with chemical and geometrical functionalities [51]. POSS is a molecule of generic formula $Si_nO_{1.5n}$ composed of eight silicon atoms forming a cage of 0.53 nm diameter [53]. The functionality and size of the groups attached to Si atoms can be varied according to the required applications (copolymerization and blending) [54,55]. In particular, various types of organic chains can be

attached to the POSS cage, which can modify its solubility in different polymers, providing a better dispersion in the matrix [56]. The groups attached to the Si atoms of POSS can be used to enhance the compatibility with the host polymer taking benefit of the properties of inorganic nanoparticles [57]. POSS, when grafted with reactive functional groups, can be copolymerized with more conventional monomers. The resulting organic-inorganic hybrid is expected to have enhanced properties compared to the organic homopolymer, such as an increased specific surface, and a larger flexibility [58,59]. POSS-related materials meet applications in polymer based electrolytes [60,61], biomaterials [62,63], hybrid nanocomposites [64], polymer-based optoelectronic devices [65], and sensitivity enhancers in vapour sensing application [51]. In order to maximize the effect of POSS it was decided to incorporate it directly in the polymer chains from the matrix. Poly(styrene) (PS) and poly(methyl methacrylate) (PMMA) were selected because of their amorphous nature, which is known to increase their permeability to vapours and, thus, decrease the response time of the derived transducers [21]. Of course, the second criteria was their ability to be copolymerized with reactive POSS. Moreover Wu et al. showed that PS-co-POSS did not crystallize, even generating additional free volume, leading to a higher level of plasticization of the matrix [63,66–68]. A similar behaviour was observed with PMMA-co-POSS that exhibited a very low crystallinity [69] and presented a decreased T_g compared to the homopolymer [70]. Therefore, the introduction of POSS in CNT-based CPC is expected to boost their sensitivity [51] by modifying the molecular mobility of polymers without causing any segregation thanks to their copolymerization in the same chain. The cage structure of POSS molecules and their tailorable organic functionalities should also provide additional means of discrimination of vapours, complementary to those resulting from molecular interaction of analytes with polymer chains and carbon nanotubes. To validate these assumptions, solutions of CNT co-dispersed with poly(POSS-co-styrene), and poly(POSS-co-methyl methacrylate) have been synthesized, then sprayed layer-by-layer (sLbL) on microelectrodes to characterized their chemo-resistive behaviour when exposed to ammonia and formaldehyde vapours.

2. Experimental

2.1. Materials

Multi-walled carbon nanotubes (CNT) were obtained from Nanocyl SA, Sambreville, Belgium. MWCNT were prepared by catalytic carbon vapour deposition (CCVD) method. They have 90% purity, average diameters of 9.5 nm, and average lengths of 1.5 microns. MWCNT were used without any purification. Poly(methyl methacrylate) (PMMA) was VQ 101S from Rhöm (Munich, Germany). Flakes of atactic poly(styrene) (aPS) were purchased from Polyscience (Paris, France) with an average molar mass of M_n = 50,000 g·mol^{-1}. Poly[(propyl-methacryl-hepta isobutyl-PPS)-co-styrene], or PS-co-POSS, and poly[(propyl-methacryl-hepta isobutyl-PPS)-co-methyl methacylate], or PMMA-co-POSS, were procured from Sigma-Aldrich (St. Louis, MO, USA). Both copolymers contain 45 wt% of POSS (about 7 mol%), randomly distributed in the polymer chain. All solvents and chloroform used in the experiments were also obtained from Sigma-Aldrich (St. Louis, MO, USA).

2.2. Sensor's Fabrication and Chemo-Resistive Characterization

Quantum resistive vapour sensors (vQRS) were prepared by spraying layer-by-layer (sLbL) method using dispersion of copolymer and CNT in chloroform. Two dispersions were prepared by sonication (Branson 3800) of each copolymer with 2 wt% CNT in chloroform to reach the concentration of 10 g·dm^{-3}. Four layers of these two dispersions were sprayed over interdigitated electrodes. The resulting initial resistances were R_0 = 17.9 ± 3 kΩ and R_0 = 21.6 ± 5 kΩ for PS-co-POSS/CNT and PMMA-co-POSS/CNT, respectively.

The chemo-resistive properties were analysed by recording the change in the electrical resistance for both sensors. vQRS were exposed to five minutes' alternative cycles of nitrogen and vapours (formaldehyde or ammonia). These vapours were generated by an OVG4 (Owlstone Ltd., Cambridge, UK) oven using calibrated permeation tubes of ammonia (NH$_3$) and formaldehyde (CH$_2$O) at 100 cm^3·min^{-1}, then sent to the sensor chamber for testing. The concentration of vapours in the outlet

of the oven was varied using a split flow controller from 100 ppm (parts per million) to 500 ppb (parts per billion). Two different copolymers of POSS were used to investigate the effects of the polymer chemical nature and physico-chemical structure on vQRS chemo-resistive characteristics. The change in electrical resistance of sensors was measured by Keithley 6517 and recorded by a program made with the Labview software (National Instruments, Nanterre, France). The response of the vQRS was expressed as relative amplitude (A_R) given in Equation (1):

$$A_R = \frac{R - R_0}{R_0}$$ (1)

where R_0 is the initial resistance of sensors in a dry nitrogen stream and R is the resistance in the presence of pure or solvent-water vapour mix.

In order to assess the efficiency of the sensors in the ppm to ppb concentration range, the signal-to-noise ratio (SNR) during exposure of VOC is calculated with Equation (2) according to [71]:

$$SNR = \Delta R_{max} / \sigma_{baseline}$$ (2)

where ΔR_{max} defines the maximum resistance change upon exposing the sensor to analyte, $\sigma_{baseline}$ represents the standard deviation in baseline resistance before analyte delivery, calculated using at least 10 data points.

The nanoscale characterizations were done by atomic force microscopy (AFM) in ambient conditions using the light tapping mode (TM-AFM) on a calibre multimode scanning probe microscope from Bruker-Veeco, Paris, France. The morphology of POSS-CNT sensors was observed under the Zeiss EVO 50 scanning electronic microscope (SEM). A scheme summarizing the vQRS processing and chemo-resistive sensing characterization is illustrated in Figure 2.
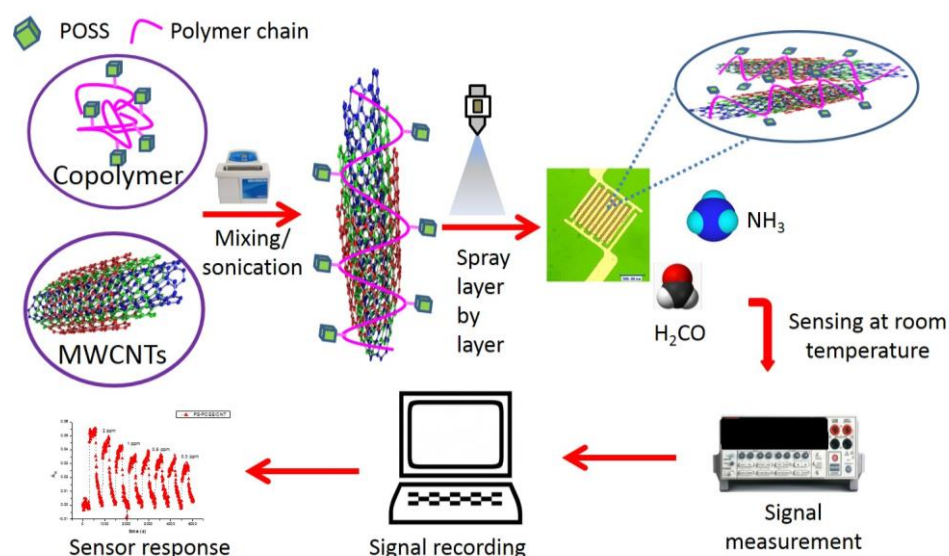

Figure 2. Scheme of the development, assembly, fabrication, and chemo-resistive characterization of quantum resistive vapour sensors (vQRS).

3. Results and Discussion

3.1. vQRS Morphological Characterization

The fabrication of POSS copolymer-functionalized CNT vQRS starts by the LbL spraying of nanocomposite suspensions on interdigitated electrodes to structure, step-by-step, the transducer from the nano to the microscale. In Figure 3a a SEM profile allows evaluating the average thickness of the transducing films made of four layers was about 4 μm and also shows the porous nature of transducers which is also visible from the top image in the Figure 3b. In Figure 3c,d, the AFM images of, respectively, PMMA-co-POSS copolymer and its nanocomposite with CNT show the homogeneity of the copolymer film and the good coating and dispersion of one CNT in the matrix. A second level

of porosity (80 nm) can also be observed from these two AFM pictures revealing another characteristic of sLbL-structured transducers expected to favour analyte molecule diffusion to the CNT nanojonctions. POSS molecules are not visible in these pictures, suggesting that they are not aggregated, as it was shown that they tend to assemble in catenary nanoclusters [72].
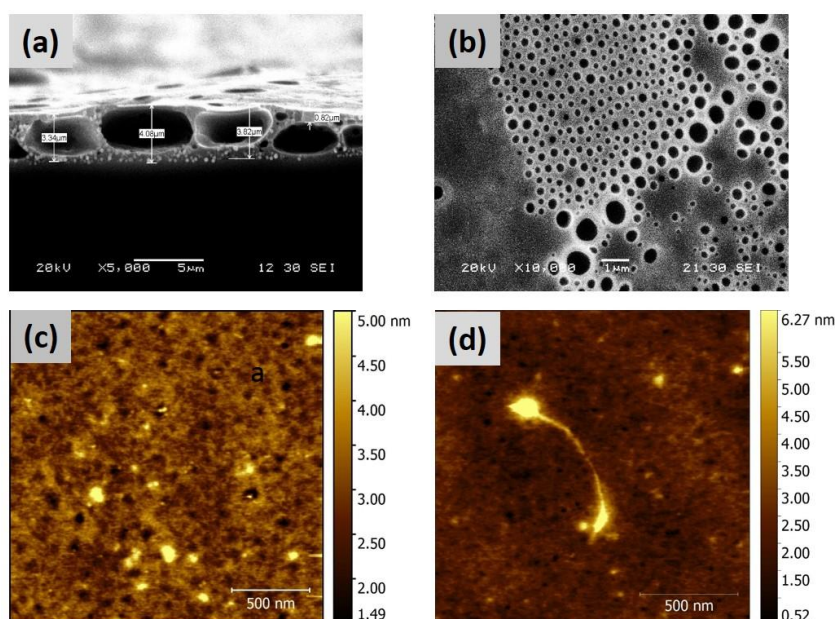

Figure 3. (**a**) SEM image of the nanocomposite transducing film's cross section; (**b**) SEM image of transducers' surface; (**c**) AFM image of PMMA-co-POSS copolymer; and (**d**) AFM image of nanocomposite showing CNT in the copolymer matrix.

Porosity is promoting the analytes' diffusion within the CPC transducers leading to shorter response times as pointed out earlier for PS-CNP-based vQRS [73]. The different nature of the two copolymers of POSS were used to investigate the effects of the chemical interactions and physico-chemical structure on vQRS chemo-resistive characteristics. It is expected that the junctions of the random network of CNT are coated with the synthesized nanocomposite in order to provide effective chemo-sensitive nanoswitches acting on tunnelling conduction in the presence of analytes. The molecular mobility of chains at room temperature (20 °C) is expected to facilitate the disconnection of junctions due to the local swelling induced by the CH_2O and NH_3 vapour molecules. The amorphous nature of both PS-co-POSS and PMMA-co-POSS matrices having glass transition temperatures (T_g), respectively, 20 °C below and slightly above 100 °C, as can be seen from Table 2, is the guarantee of low density and absence of a gas barrier, such as crystalline lamellae. Nevertheless, comparing the data obtained in the present work to others found in the literature does not allow concluding on any strong effect of either CNT of POSS on the T_g of PMMA or PS. At least the effect of these nanofillers is in the same order of magnitude as that of the molar mass.

Table 2. The effect of nanofillers on nanocomposite glass temperature transitions T_g.

Material	T_g (°C)
PS (M_n = 50,000 g·mol^{-1})	100 [73]
PMMA (M_n = 3.9 × 10^4 g·mol^{-1})	100.2 [74]
PS-1% *w/w* CNT	105 [75]
PMMA-5% *w/w* CNT	102.5 [74]
PS-co-POSS/2% *w/w* CNT	80.7 [this work]
PMMA-co-POSS/2% *w/w* CNT	112.7 [this work]

3.2. vQRS Chemo-Resistive Characterization

3.2.1. Effect of POSS on the Chemo-Resistive Response?

If no strong effect of POSS on the polymer matrices' morphologies can be noticed, it is not the case that their chemo-resistive responses are associated to CNT, as is clearly visible in Figure 4. POSS molecules bring a clear boosting effect to the chemo-resistive responses of all CPC transducers. as already found in a previous work on CNT-based vQRS [51].
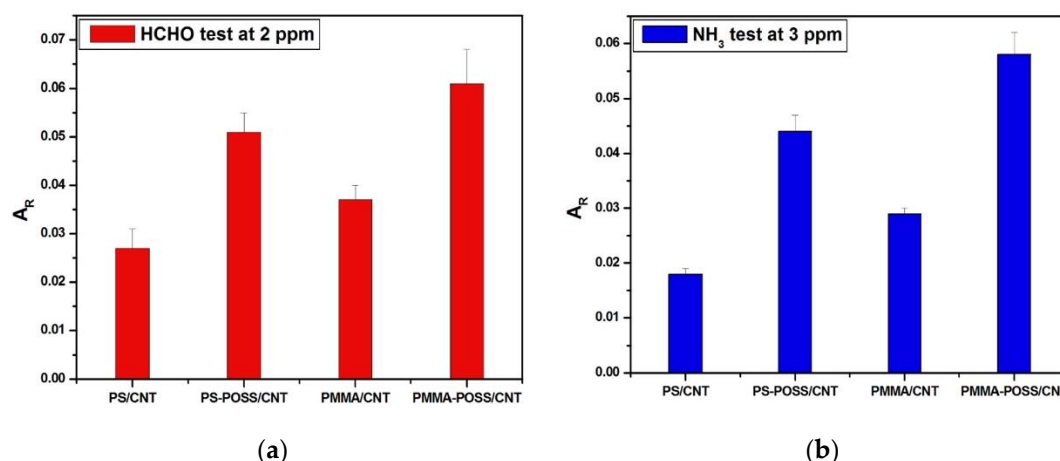

(**a**)   (**b**)

Figure 4. The effect of the presence of POSS co-monomer on the chemo-resistive responses of PS-CNT and PMMA-CNT sensors to (**a**) 2 ppm of CH$_2$O vapour and (**b**) 3 ppm of NH$_3$ vapour.

When exposed to 2 ppm of formaldehyde vapours PS-CNT and PMMA-CNT vQRS see their responses increasing by 88% and 64%, respectively, by the introduction of POSS, through the substitution of undoped polymer nanocomposites by PS-co-POSS-CNT and PMMA-co-POSS-CNT. The same conclusion can be made when the vQRS are exposed to 3 ppm of ammonia vapour. Compared to undoped polymers, the addition of POSS boosts the responses of 114% and 100% for PS-CNT and PMMA-CNT, respectively. These results confirm that POSS can effectively enhance the CNT network's disconnection thanks to a spacing effect that can favour the diffusion of analyte molecules to the junctions.

3.2.2. Principle of CH$_2$O and NH$_3$ Detection with vQRS

The sensing mechanism of vQRS is rather different from that of metal oxide or semiconductor-based sensors; it is based on the disconnection of the conductive architecture (at nanojunctions) resulting from the adsorption of vapour molecules both on carbon nanofillers and inside the amorphous phase of the polymer matrix (there is a partial swelling of the macromolecules coating the nanojunctions) [76,77]. By increasing the average gap ΔZ between CNT, the vapour molecules generate tunnelling conduction that yield exponential variations of the global resistance of transducers [23,78], according to Equation (3), this is why these sensors are called quantum resistive vapour sensors vQRS [21,51]:

$$A_r = ae^{b\Delta Z} \tag{3}$$

where *Ar* is the relative variation of resistivity, and *a* and *b* are positive constants and ΔZ the gap variation between two vicinal CNT (typically $1 < \Delta Z < 10$ nm).

The selectivity of such vQRS results from van der Waals interactions between the organic component of the nanocomposite present at junctions and the analytes, which are well modelled by the χ_{12} intermolecular interaction parameter from Flory-Huggins that can be calculated with Equation (4):

$$\chi_{12} = \frac{V_m}{RT} \ (\delta_{Tlink} - \delta_{Tana})^2 \tag{4}$$

where V_m is the molar volume of the solvent (cm^3·mol^{-1}), T is the temperature (K), the ideal gas constant ($R = 8.314$ J·mol^{-1}), and the analyte and linker global solubility parameters δ_{Tana} and δ_{Tlink} (J$^{1/2}$·cm$^{-3/2}$), respectively.

The closest to zero χ_{12} is, the highest the interactions between polymer chains and organic molecules and consequently the largest the swelling of junctions and the disconnection ability. Finally the response amplitude of vQRS can be well related to $1/\chi_{12}^n$, as described in a previous work [77] and expressed in Equation (5):

$$A_r = a.\, e^{\frac{b}{\chi_{12}^n}} \tag{5}$$

where χ_{12} is the Flory-Huggins intermolecular interaction parameter which can be determined using Equation (4) and *a* and *b* are constants

This model is meaningful to link the chemo-resistive properties to the chemical structure of the vQRS constituents.

For example, by using the Hansen's solubility parameters from Table 3 yields the values of χ_{12} collected in Table 4. These results predict well that the lower the χ_{12} the larger the chemo-resistive response A_r. It seems however more difficult to predict the effect of POSS molecules in the selectivity of transducers, as they may act distinctly to enhance the disconnectability by space effect.

Table 3. Hansen's solubility parameters of the organic compounds possibly interacting in the vQRS using $\delta_t = (\delta_D^2 + \delta_P^2 + \delta_H^2)^{1/2}$.

Compound	δ_D (MPa$^{1/2}$)	δ_P (MPa$^{1/2}$)	δ_H (MPa$^{1/2}$)	δ_t (MPa$^{1/2}$)	V_m (cm^3·mol^{-1})
NH$_3$	13.7	16.7	18.8	28.63	25
C$_2$HO	12.8	14.4	15.4	24.66	36.9
PS	5.9	18.7	3.5	19.92	-
PMMA	10.5	18.8	5.7	22.27	-

Table 4. Flory-Huggins intermolecular interactions parameters.

χ_{12}/A_r	PS	PMMA
NH$_3$	0.765/0.018	0.407/0.028
CH$_2$O	0.334/0.026	0.085/0.036

As the boosting effect of POSS on the responses of both PS-CNT and PMMA-CNT to CH$_2$O and NH$_3$ was demonstrated at the ppm level, only the performances of these two sensors will be tested under more severe conditions in the following sections.

3.2.3. Formaldehyde Sensing with PS-co-POSS/CNT and PMMA-co-POSS/CNT

As mentioned earlier, CH$_2$O is a dangerous vapour even at low concentrations. Therefore, CH$_2$O vapours were generated by an OVG4 oven at concentrations ranging from 0.3 ppm to 27 ppm, and carried by a 100 cm^3·min^{-1} nitrogen flow to sensors' chamber. The two different selected vQRS, PS-co-POSS/CNT and PMMA-co-POSS/CNT, were exposed to CH$_2$O nitrogen/analyte successive cycles of 5 min in order to interpret the responses collected in Figure 5a. The shape of the two curves appears very typical of the LHC model developed to fit the evolution of the chemo-resistive response with the concentration of the analyte and is expressed in Equation (6) [23,79,80]. The LHC model also allows deducing whether penetrating solvent vapour molecules will only slightly adsorb on specific sites (Langmuir), diffuse and form of several layers of vapour molecules on CPC (Henry), or generate plasticization and swelling of the matrix through the clustering of solvent vapour molecules (Clustering). Each of these three terms is expressed in Equation (6):

$$A_r = \frac{b_L(f'' - f)f}{1 + b_L} + k_H f + (f - f')f^{n'} \tag{6}$$

where b_L is the Langmuir affinity constant, f is the solvent fraction, f' is the solvent fraction over which clustering starts, f'' is the vapour fraction over which Langmuir's diffusion replaced by Henry's diffusion, k_H is Henry's solubility coefficient, and n' is the number of vapour molecules associated in clusters.

According to this model, and the shape of the two curves plotted in Figure 5a, it is possible to state that between 0.3 ppm and 5 ppm the chemo-resistive behaviours resulting from the interactions of molecules with the CNT network fits a Langmuir adsorption, whereas between 5 ppm and 27 ppm it is more coherent with Henry's diffusion. These data demonstrate the capability of both vQRS to detect sub ppm amounts of CH_2O vapours (300 ppb) and this good signal to noise ratio, i.e., SNR = 17 and 16 for PMMA-co-POSS/CNT and PS-co-POSS/CNT, respectively. Additionally, the PMMA-based vQRS appears more sensitive at concentrations, i.e., under 15 ppm, than its PS homologue, but this tendency seems to be reversed over 15 ppm due to a larger Henry's diffusion coefficient of the latter (in the second term of Equation (6) the slope is proportional to k_H). Under 5 ppm according to the first term of the same equation, the slope of the curves presented in Figure 5b is proportional to b_L, the Langmuir's affinity constant. Actually, b_L is also expressing the sensitivity at low concentration, which was evaluated by a linear fit for PS-co-POSS/CNT and PMMA-co-POSS/CNT to, respectively, 0.011 ppm^{-1} and 0.014 ppm^{-1} with R^2 = 0.996 and 0.992.
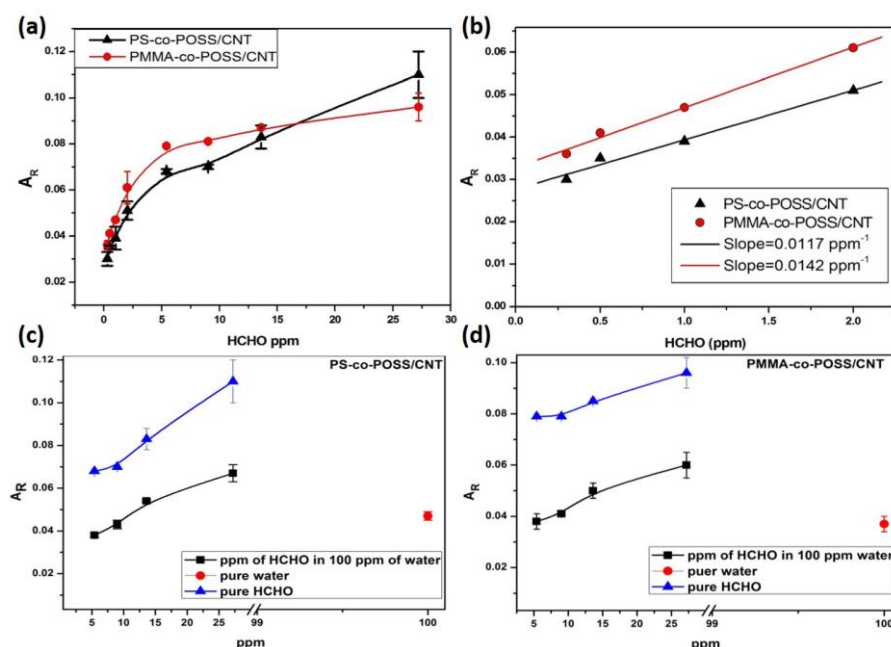

Figure 5. (**a**) PS-co-POSS/CNT and PMMA-co-POSS/CNT sensors response towards CH_2O; and (**b**) sensitivity of both sensors towards CH_2O, and CH_2O sensing in presence of 100 ppm of water by (**c**) PS-co-POSS/CNT and (**d**) PMMA-co-POSS/CNT sensors respectively.

The effect of water molecules on the detection of analytes makes sense since they are present almost everywhere in the atmosphere in rather large amounts and can even combine with analytes. To study this fact, CH_2O detection was carried out in the presence of water to test the capability of both vQRS to detect toxic vapours in harsh conditions. Thus, CH_2O concentration was varied from 5 ppm to 27 ppm in the presence of 100 ppm of water, and the results are presented in Figure 5c,d. It can be seen that both sensors were able to detect very low contents of target analytes in a humidified environment, despite a global decrease in the amplitude of their responses. This can be explained by the fact that CH_2O can be partly soluble in water, and that the two molecules are competing for the adsorption on the sensor's nanojunctions responsible for the chemo-resistive response. However, at ambient temperature (T_{amb} = 20 °C), and in the presence of 100 ppm of water, it is remarkable that both PS-co-POSS/CNT and PMMA-co-POSS/CNT sensors were able to detect 14 ppm and 9 ppm of CH_2O, respectively proving their robustness against moisture.

3.2.4. Ammonia Sensing with PS-co-POSS/CNT and PMMA-co-POSS/CNT

PS-co-POSS/CNT and PMMA-co-POSS/CNT vQRS were also exposed to ammonia, the second important toxic vapour of our study, under similar conditions as for CH_2O. NH_3 vapours were generated by the OVG4 oven through a membrane previously calibrated at concentrations ranging from 500 ppb to 3 ppm in a nitrogen stream of 100 $cm^3 \cdot min^{-1}$. This narrower range of concentrations was due to operating limits of the device in particular the permeation tube and the oven temperature. Nevertheless, is was possible to record the chemo-resistive signals of both sensors that were found to respond quickly to 3 ppm pulses of NH_3, i.e., within 5 s with an increase of up to 4–6%, as seen in Figure 6a,b. As expected A_R was gradually decreasing with the concentration of NH_3, but was large enough to allow the measurement with the satisfying SNR values of respectively 10 and 13 for PMMA-co-POSS/CNT and PS-co-POSS/CNT. The sensitivity of sensors determined by a linear fit in Figure 6c was also found to decease accordingly, i.e., 6.2×10^{-3} ppm^{-1} for PS-co-POSS/CNT and 7.8×10^{-3} ppm^{-1} for PMMA-co-POSS/CNT with R^2 = 0.996 and 0.992 respectively. However, this sensitivity is comparable to that obtained by JOULAZADEH et al. [81] for sensors based on poly(pyrrole) 3.3×10^{-3} ppm^{-1} and for poly(pyrrole)-SnO_2 7.9×10^{-3} ppm^{-1}.
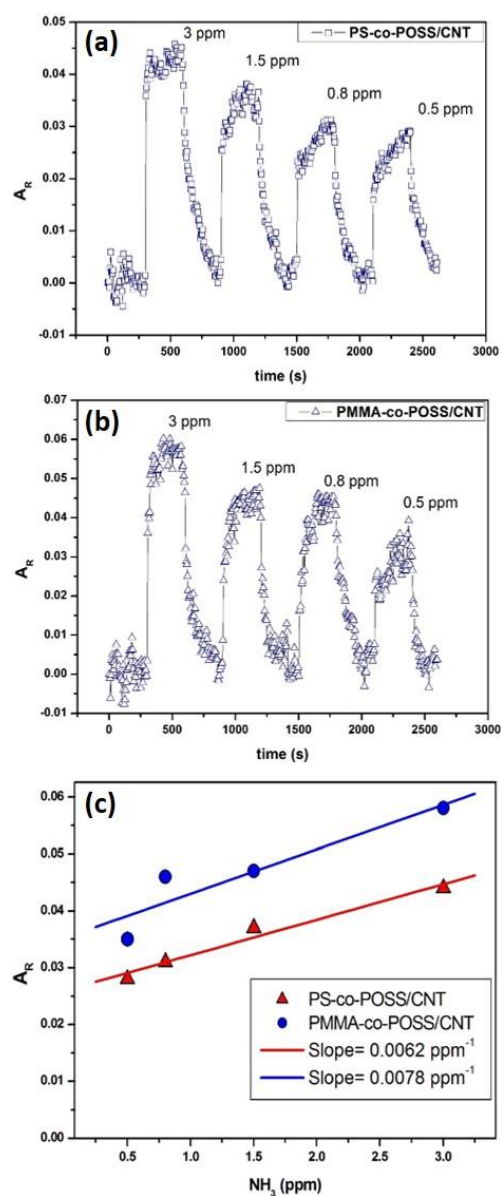

Figure 6. The effect of the addition of 100 ppm on (**a**) PS-co-POSS/CNT and (**b**) PMMA-co-POSS/CNT sensors' responses when exposed to varying concentrations of NH_3, and (**c**) their sensitivity determination towards NH_3.

Figure 7a,b summarizes the influence of the presence of 100 ppm of water on the detection of NH_3 molecules by the two sensors. It can be seen that, despite the decreasing values of A_R due to the presence of H_2O, PMMA-co-POSS/CNT and PS-co-POSS/CNT were still able to detect 1.5 ppm and 3 ppm of NH_3. However, the fact that the two curves are merging at about 500 ppb of NH_3 in Figure 7a suggests that-PS based sensors will not be able to properly discriminate NH_3 under its pure form and when strongly hydrated.
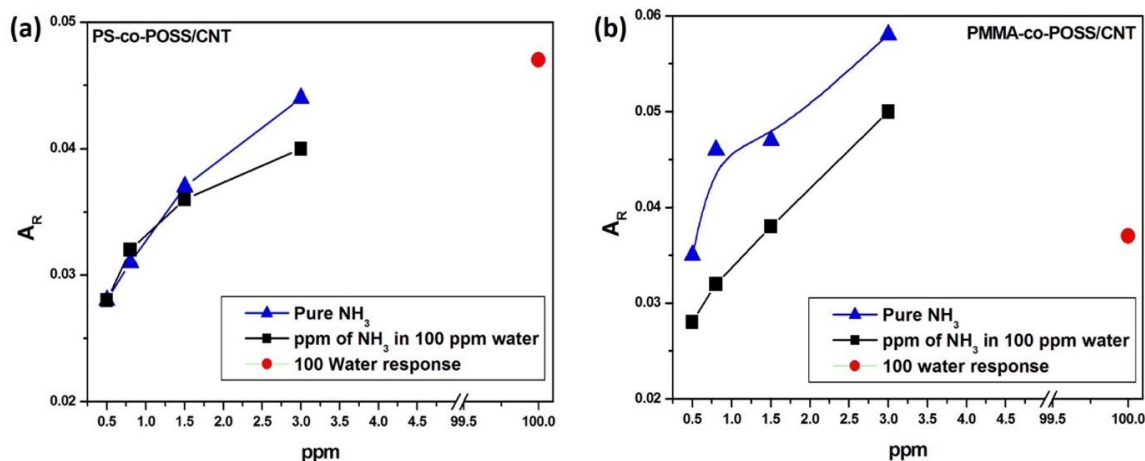

Figure 7. Summary of the effect of the presence of 100 ppm of water on the chemo-resistive responses of (**a**) PS-co-POSS/CNT and (**b**) PMMA-co-POSS/CNT when exposed to NH_3.

4. Conclusions

Quantum resistive vapour sensors made of a CNT conducting architecture functionalized by POSS-hybridized PMMA and PS matrices, were nanostructured by spraying layer-by-layer to detect vapours that can be toxic at only some tens of ppb. SEM and AFM characterized the interest of this processing technique to generate micro- and nanopores facilitating the analytes' diffusion to the nanojunctions and, thus, the quickness of the sensors' responses. Both types of vQRS were exposed, firstly, to ppm amounts of NH_3 and CH_2O to confirm the boosting effect of the introduction of polyhedral oligomeric silsesquioxane on the chemo-resistive response of the sensors. Then PMMA-co-POSS/CNT and PS-co-POSS/CNT were exposed to pulses of very small amounts of ammoniac and formaldehyde vapours ranging from 300 ppb to 100 ppm to demonstrate their limit of detection. At the minimum fraction of molecules allowed by our device, i.e., 0.3 ppm, both vQRS had a SNR of about 15, which was still enough to allow for good measurements. In agreement with the Langmuir-Henry-clustering model developed to fit electro-sorption experiments, it was possible to identify that both vQRS had a chemo-resistive behaviour driven by Langmuir adsorption between 0.3 ppm and 15 ppm and by Henry's diffusion between 15 ppm and 100 ppm. In degraded conditions the two sensors exhibited decreasing values of their A_R due to the presence of 100 ppm additional moisture, but PMMA-co-POSS/CNT and PS-co-POSS/CNT were still able to detect 1.5 ppm and 3 ppm of NH_3. All POSS-based vQRS have demonstrated their fast response, ability to detect ppb concentrations of NH_3 and CH_2O toxic gases, and to work at room temperature in a humid atmosphere. The POSS molecules were assumed to increase the sensing ability of the sensors, without much changing their selectivity due to their action as nanospacers within the conducting network that gave more mobility to macromolecules and more space for analytes to diffuse. The PMMA-co-POSS/CNT sensor was slightly more sensitive than the PS-co-POSS/CNT sensors, but both of them could be good candidates for integration into an e-nose designed for air quality and volatolomics monitoring.

Author Contributions: A.S., M.C., V.C. and J.F.F. conceived and designed the experiments; A.S. performed the experiments; A.S., M.C., V.C. and J.F.F. analyzed the data; A.S., M.C. and V.C. contributed reagents/materials/analysis tools; A.S., M.C. and J.F.F. wrote the paper.

Conflicts of Interest: The authors declare no conflict of interest.

References

1. Lindmeier, C.; Osseiran N.; Chriscaden, K. *An Estimated 12.6 Million Deaths Each Year are Attributable to Unhealthy Environments*; World Health Organization: Geneva, Switzerland, 2016.

2. Cancer today: Population fact sheets, world estimated incidence and mortality of cancer, Fact Sheet. 2012. Available online: http://globocan.iarc.fr/Pages/fact_sheets_population.aspx (accessed on 11 July 2017).

3. Broza, Y.Y.; Kremer, R.; Tisch, U.; Gevorkyan, A.; Shiban, A.; Best, L.A. A nanomaterial-based breath test for short-term follow-up after lung tumor resection. *Nanomed. Nanotechnol. Biol. Med.* **2013**, *9*, 15–21.

4. Broza, Y.Y.; Zuri, L.; Haick, H. Combined volatolomics for monitoring of human body chemistry. *Sci. Rep.* **2014**, *4*, 1–6.

5. Hashim, D.; Boffetta, P. Occupational and environmental exposures and cancers in developing countries. *Ann. Glob. Health* **2014**, *80*, 393–411.

6. Mount, G.H.; Rumburg, B.; Havig, J.; Lamb, B.; Westberg, H.; Yonge, D. Measurement of atmospheric ammonia at a dairy using differential optical absorption spectroscopy in the mid-ultraviolet. *Atmos. Environ.* **2002**, *36*, 1799–1810.

7. Pijolat, C.; Pupier, C.; Sauvan, M.; Tournier, G.; Lalauze, R. Gas detection for automotive pollution control. *Sens. Actuators B Chem.* **1999**, *59*, 195–202.

8. Kohl, D. Function and applications of gas sensors. *J. Phys. D Appl. Phys.* **2001**, *34*, R125.

9. Ampuero, S.; Bosset, J.O. The electronic nose applied to dairy products: A review. *Sens. Actuators B Chem.* **2003**, *94*, 1–12.

10. Greenstein, G.R. The Merck Index: An Encyclopedia of Chemicals, Drugs, and Biologicals (14th edition). *Ref. Rev.* **2006**, *21*, 40.

11. Zakrzewska, K. Mixed oxides as gas sensors. *Thin Solid Films* **2001**, *391*. 229–238.

12. Wojkiewicz, J.L.; Bliznyuk, V.N.; Carquigny, S.;Elkamchi, N.; Redon, N.; Lasri, T. Nanostructured polyaniline-based composites for ppb range ammonia sensing. *Sens. Actuators B Chem.* **2011**, *160*, 1394–1403.

13. Peeters, R.; Berden, G.; Apituley, A.; Meijer, G. Open-path trace gas detection of ammonia based on cavity-enhanced absorption spectroscopy. *Appl. Phys. B* **2000**, *71*, 231–236.

14. Tiggelaar, R.M.;Veenstra, T.T.; Sanders, R.G.P.; Berenschot, E.; Gardeniers, H.; Elwenspoek, M. Analysis systems for the detection of ammonia based on micromachined components modular hybrid versus monolithic integrated approach. *Sens. Actuators B Chem.* **2003**, *92*, 25–36.

15. Winquist, F.; Spetz, A.; Lundström, I.; Danielsson, B. Determination of ammonia in air and aqueous samples with a gas-sensitive semiconductor capacitor. *Anal. Chim. Acta* **1984**, *164*, 127–138.

16. Xu, C.N.; Miura, N.; Ishida, Y.; Matsuda, K.; Yamazoe, N. Selective detection of NH_3 over NO in combustion exhausts by using Au and MoO_3 doubly promoted WO_3 element. *Sens. Actuators B Chem.* **2000**, *65*, 163–165.

17. Cantalini, C. Valentini, L.; Armentano, I.; Lozzi, L.; Kenny, J.M.; Santucci, S. Sensitivity to NO_2 and cross-sensitivity analysis to NH_3, ethanol and humidity of carbon nanotubes thin film prepared by PECVD. *Sens. Actuators B Chem.* **2003**, *95*, 195–202.

18. Arab, M.; Berger, F.; Picaud, F.; Ramseyer, C.; Glory, J.; Mayne-L'Hermite, M. Direct growth of the multi-walled carbon nanotubes as a tool to detect ammonia at room temperature. *Chem. Phys. Lett.* **2006**, *433*, 175–181.

19. Battie, Y.; Ducloux, O.; Thobois, P.; Dorval, N.; Lauret, J.S.; Attal-Trétout, B. Gas sensors based on thick films of semi-conducting single walled carbon nanotubes. *Carbon N. Y.* **2011**, *49*, 3544–3552.

20. Feller, J.F.; Gatt, N.; Kumar, B.; Castro, M. Selectivity of chemoresistive sensors made of chemically functionalized carbon nanotube random networks for volatile organic compounds (VOC). *ChemoSensors* **2014**, *2*, 26–40.

21. Kumar, B.; Castro, M.; Feller, J.F. Quantum resistive vapour sensors made of polymer coated carbon nanotubes random networks for biomarkers detection. *Chem. Sens.* **2013**, *3*, 1–7.

22. Li, Y.; Wang, H.; Yang, M. n-Type gas sensing characteristics of chemically modified multi-walled carbon nanotubes and PMMA composite. *Sens. Actuators B Chem.* **2007**, *121*, 496–500.

23. Kumar, B.; Feller, J.F.; Castro, M.; Lu, J. Conductive bio-Polymer nano-Composites (CPC): Chitosan-carbon

nanotube transducers assembled via spray layer-by-layer for volatile organic compound sensing. *Talanta* **2010**, *81*, 908–915.

24. Kumar, B.; Castro, M.; Feller, J.F. Poly(lactic acid)–multiwall carbon nanotube conductive biopolymer nanocomposite vapour sensors. *Sens. Actuators B Chem.* **2012**, *161*, 621–628.

25. Huyen, D.N.; Tung, N.T.; Vinh, T.D.; Thien, N.D. Synergistic effects in the gas sensitivity of polypyrrole/single wall carbon nanotube composites. *Sensors* **2012**, *12*, 7965–7974.

26. Van Hieu, N.; Dung, N.Q.; Tam, P.D.; Trung, T.; Chien, N.D. Thin film polypyrrole/SWCNTs nanocomposites-based NH_3 sensor operated at room temperature. *Sens. Actuators B Chem.* **2009**, *140*, 500–507.

27. Setka, M.; Drbohlavova, J.; Hubalek, J. Nanostructured polypyrrole-based ammonia and volatile organic compound sensors. *Sensors* **2017**, *17*, 562.

28. Sharma, S.; Hussain, S.; Singh, S.; Islam, S.S. MWCNT-conducting polymer composite based ammonia gas sensors: A new approach for complete recovery process. *Sens. Actuators B Chem.* **2014**, *194*, 213–219.

29. Huotari, J.; Lappalainen, J.; Eriksson, J.; Bjorklund, R.; Heinonen, E.; Miinalainen, I. Synthesis of nanostructured solid-state phases of V_7O_{16} and V_2O_5 compounds for ppb-level detection of ammonia. *J. Alloy. Compd.* **2016**, *675*, 433–440.

30. Krivetskiy, V.; Malkov, I.; Garshev, A.; Mordvinova, N.; Lebedev, O.I.; Dolenko, S. Chemically modified nanocrystalline SnO_2-based materials for nitrogen-containing gases detection using gas sensor array. *J. Alloy. Compd.* **2017**, *691*, 514–523.

31. Dalavi, D.S.; Harale, N.S.; Mulla, I.S.; Rao, V.K.; Patil, V.B.; Kim, I.Y. Nanoporous network of nickel oxide for ammonia gas detection. *Mater. Lett.* **2015**, *146*, 103–107.

32. Kwon, O.S.; Hong, J.Y.; Park, S.J.; Jang, Y.; Jang, J. Resistive gas sensors based on precisely size-controlled polypyrrole nanoparticles: Effects of particle size and deposition method. *J. Phys. Chem. C* **2010**, *114*, 18874–18879.

33. Xiang, C.; Jiang, D.; Zou, Y.; Chu, H.; Qiu, S.; Zhang, H. Ammonia sensor based on polypyrrole-graphene nanocomposite decorated with titania nanoparticles. *Ceram. Int.* **2015**, *41*, 6432–6438.

34. Korpan, Y.I.; Gonchar, M.V.; Sibirny, A.A.; Martelet, C.; El'skaya, A.V.; Gibson, T.D. Development of highly selective and stable potentiometric sensors for formaldehyde determination. *Biosens. Bioelectron.* **2000**, *15*, 77–83.

35. Kawamura, K.; Kerman, K.; Fujihara, M.; Nagatani, N.; Hashiba, T.; Tamiya, E. Development of a novel hand-held formaldehyde gas sensor for the rapid detection of sick building syndrome. *Sens. Actuators B Chem.* **2005**, *105*, 495–501.

36. Que, Z.; Furuno, T.; Katoh, S.; Nishino, Y. Evaluation of three test methods in determination of formaldehyde emission from particleboard bonded with different mole ratio in the urea-formaldehyde resin. *Build. Environ.* **2007**, *42*, 1242–1249.

37. An, J.Y.; Kim, S.; Kim, H.J.; Seo, J. Emission behavior of formaldehyde and TVOC from engineered flooring in under heating and air circulation systems. *Build. Environ.* **2010**, *45*, 1826–1833.

38. World Health Organization (WHO). Air quality guidelines for Europe. *Environ. Sci. Pollut. Res.* **1996**, *3*, 23–23.

39. U.S. Dept Health & Human Services. *Occupational Safety and Health Guideline for Formaldehyde Potential Human Carcinogen*; NIOSH: Washington, DC, USA, 1988.

40. Suzuki, Y.; Nakano, N.; Suzuki, K. Portable sick house syndrome gas monitoring system based on novel colorimetric reagents for the highly selective and sensitive detection of formaldehyde. *Environ. Sci. Technol.* **2003**, *37*, 5695–5700.

41. Achmann, S.; Hermann, M.; Hilbrig, F.; Jérôme, V.; Hämmerle, M.; Freitag, R. Direct detection of formaldehyde in air by a novel NAD+- and glutathione-independent formaldehyde dehydrogenase-based biosensor. *Talanta* **2008**, *75*, 786–791.

42. Lv, P.; Tang, Z.A.; Yu, J.; Zhang, F.T.; Wei, G.F.; Huang, Z.X. Study on a micro-gas sensor with SnO_2-NiO sensitive film for indoor formaldehyde detection. *Sens. Actuators B Chem.* **2008**, *132*, 74–80.

43. Li, X.; Liu, J.; Guo, H.; Zhou, X.; Wang, C.; Sun, P. Au@In_2O_3 core-shell composites: A metal-semiconductor heterostructure for gas sensing applications. *RSC Adv.* **2015**, *5*, 545–551.

44. Barsan, N.; Koziej, D.; Weimar, U. Metal oxide-based gas sensor research: How to? *Sens. Actuators B Chem.* **2007**, *121*, 18–35.

45. Zhang, D.; Liu, J.; Jiang, C.; Liu, A.; Xia, B. Quantitative detection of formaldehyde and ammonia gas via metal oxide-modified graphene-based sensor array combining with neural network model. *Sens. Actuators B Chem.* **2017**, *240*, 55–65.

46. Zhang, D.; Jiang, C.; Li, P.; Sun, Y. Layer-by-layer self-assembly of Co_3O_4 nanorod-decorated MoS_2 nanosheet-based nanocomposite toward high-performance ammonia detection. *ACS Appl. Mater. Interfaces* **2017**, *9*, 6462–6471.

47. Fang, F.; Bai, L.; Sun, H.; Kuang, Y.; Sun, X.; Shi, T. Hierarchically porous indium oxide nanolamellas with ten-parts-per-billion-level formaldehyde-sensing performance. *Sens. Actuators B Chem.* **2015**, *206*, 714–720.

48. Park, H.J.; Choi, N.J.; Kang, H.; Jung, M.Y.; Park, J.W.; Park, K.H. A ppb-level formaldehyde gas sensor based on CuO nanocubes prepared using a polyol process. *Sens. Actuators B Chem.* **2014**, *203*, 282–288.

49. Güntner, A.T.; Koren, V.; Chikkadi, K.; Righettoni, M.; Pratsinis, S.E. E-Nose sensing of low-ppb formaldehyde in gas mixtures at high relative humidity for breath screening of lung cancer? *ACS Sens.* **2016**, *1*, 528–535.

50. Nag, S.; Castro, M.; Choudhary, V.; Feller, J.F. Sulfonated poly(ether ether ketone) [SPEEK] nanocomposites based on hybrid nanocarbons for the detection and discrimination of some lung cancer VOC biomarkers. *J. Mater. Chem. B Biol. Med.* **2017**, *5*, 348–359.

51. Nag, S.; Sachan, A.; Castro, M.; Choudhary, V.; Feller, J.F. Spray layer-by-layer assembly of POSS functionalized CNT quantum chemo-resistive sensors with tuneable selectivity and ppm resolution to VOC biomarkers. S*ens. Actuators B Chem.* **2016**, *222*, 362–373.

52. Feller, J.F. *Des Composites Polymères Conducteurs Aux éco-Composites Polymères*, 2nd ed.; Universitaires Européennes (EUE): Sarrebruck, Germany, 2003.

53. Zhang, W.; Müller, A.H.E. Architecture, self-assembly and properties of well-defined hybrid polymers based on polyhedral oligomeric silsequioxane (POSS). *Prog. Polym. Sci.* **2013**, *38*, 1121–1162.

54. Pielichowski, K.; Njuguna, J.; Janowski, B.; Pielichowski, J. Polyhedral oligomeric silsesquioxanes (POSS)-containing nanohybrid polymers. In *Supramolecular Polymers Polymeric Betains Oligomers*; Springer: Berlin/Heidelberg, Germany, 2006; pp. 225–296.

55. Gnanasekaran, D.; Madhavan, K.; Reddy, R.S.R. Developments of polyhedral oligomeric silsesquioxanes (POSS), POSS nanocomposites and their applications: A review. *J. Sci. Ind. Res.* **2009**, *68*, 437–464. (In India)

56. Franchini, E.; Galy, J.; Gérard, J.-F.; Tabuani, D.; Medici, A. Influence of POSS structure on the fire retardant properties of epoxy hybrid networks. *Polym. Degrad. Stab.* **2009**, *94*, 1728–1736.

57. Raftopoulos, K.N.; Pielichowski, K. Segmental dynamics in hybrid polymer/POSS nanomaterials. *Prog. Polym. Sci.* **2016**, *52*, 136–187.

58. Tanaka, K.; Adachi, S.; Chujo, Y. Structure-property relationship of octa-substituted POSS in thermal and mechanical reinforcements of conventional polymers. *J. Polym. Sci. Part A Polym. Chem.* **2009**, *47*, 5690–5697.

59. Li, S.; Simon, G.P.; Matisons, J.G. Morphology of blends containing high concentrations of POSS nanoparticles in different polymer matrices. *Polym. Eng. Sci.* **2010**, *50*, 991–999.

60. Thakur, V.K.; Ding, G.; Ma, J.; Lee, P.S.; Lu, X. Hybrid Materials and Polymer Electrolytes for Electrochromic Device Applications. *Adv. Mater.* **2012**, *24*, 4071–4096.

61. Maitra, P.; Wunder, S.L. POSS based electrolytes for rechargeable lithium batteries. *Electrochem. Solide-State Lett.* **2004**, *7*, A88.

62. Ghanbari, H.; Cousins, B.G.; Seifalian, A.M. A Nanocage for Nanomedicine: Polyhedral Oligomeric Silsesquioxane (POSS). *Macromol. Rapid Commun.* **2011**, *32*, 1032–1046.

63. Wu, J.; Mather, P.T. POSS Polymers: Physical Properties and Biomaterials Applications. *Polym. Rev.* **2009**, *49*, 25–63.

64. Fina, A.; Monticelli, O.; Camino, G. POSS-based hybrids by melt/reactive blending. *J. Mater. Chem.* **2010**, *20*, 9297–9305.

65. Nguyen, T.-P. Polymer-based nanocomposites for organic optoelectronic devices. A review. *Surf. Coat. Technol.* **2011**, *206*, 742–752.

66. Wu, J.; Haddad, T.S.; Mather, P.T. Vertex Group Effects in Entangled Polystyrene—Polyhedral Oligosilsesquioxane (POSS) Copolymers. *Macromolecules* **2009**, *42*, 1142–1152.

67. Wu, J.; Haddad, T.S.; Kim, G.-M.; Mather, P.T. Rheological Behavior of Entangled Polystyrene—Polyhedral Oligosilsesquioxane (POSS) Copolymers. *Macromolecules* **2007**, *40*, 544–554.

68. Gordon, M.; Taylor, J.S. Ideal copolymers and the second-order transitions of synthetic rubbers. i. non-crystalline copolymers. *J. Appl. Chem.* **1952**, *2*, 493–500.

69. Ma, X.-M.; Wang, B.; Zhang, M.-X.; Min, F.-F.; He, J. Synthesis and Thermal Characterizations of Pmma Nanocomposite Functionalized by Polyhedral Oligomeric Silsesquioxane, Phosphorus. *Sulfur. Silicon Relat. Elem.* **2013**, *188*, 1819–1826.

70. Kotal, A.; Si, S.; Paira, T.K.; Mandal, T.K. Synthesis of semitelechelic POSS-polymethacrylate hybrids by thiol-mediated controlled radical polymerization with unusual thermal behaviors. *J. Polym. Sci. Part A Polym. Chem.* **2008**, *46*, 1111–1123.

71. Gao, T.; Woodka, M.D.; Brunschwig, B.S.; Lewis, N.S. Chemiresistors for array-based vapor sensing using composites of carbon black with low volatility organic molecules. *Chem. Mater.* **2006**, *18*, 5193–5202.

72. Deng, H.; Skipa, T.; Zhang, R.; Lellinger, D.; Bilotti, E.; Alig, I. Effect of melting and crystallization on the conductive network in conductive polymer composites. *Polymer* **2009**, *50*, 3747–3754.

73. Feller, J.F.; Grohens, Y. Electrical response of Poly(styrene)/carbon black conductive polymer composites (CPC) to methanol, toluene, chloroform and styrene vapors as a function of filler nature and matrix tacticity. *Synth. Met.* **2005**, *154*, 193–196.

74. Tripathi, S.N.; Singh, S.; Malik, R.S.; Choudhary, V. Effect of multiwalled carbon nanotubes on the properties of poly(methyl methacrylate) in PMMA/CNT nanocomposites. *Macromol. Symp.* **2014**, *341*, 75–89.

75. Amr, I.T.; Al-Amer, A.; Al-Harthi, S.T.P.M.; Girei, S.A.; Sougrat, R. Effect of acid treated carbon nanotubes on mechanical, rheological and thermal properties of polystyrene nanocomposites. *Compos. B Eng.* **2011**, *42*, 1554–1561.

76. Kumar, B.; Castro, M.; Feller, J.F. Tailoring the chemo-resistive response of self-assembled polysaccharide-CNT sensors by chain conformation at tunnel junctions. *Carbon N. Y.* **2012**, *50*, 3627–3634.

77. Kumar, B; Castro, M.; Feller, J.F. Controlled conductive junction gap for chitosan-carbon nanotube quantum resistive vapour sensors. *J. Mater. Chem.* **2012**, *22*, 10656–10664.

78. Feller, J.F.; Castro, M.; Kumar, B. Polymer-carbon nanotube conductive nanocomposites for sensing. In *Polymer Carbon Nanotube Composites: Preparation, Properties and Applications*, 1st ed.; McNally, T., Pötschke, P., Eds.; Woodhead Publishing Limited: Cambridge, UK, 2011; pp. 760–803.

79. Bouvrée, A.; Feller, J.F.; Castro, M.; Grohens, Y.; Rinaudo, M. Conductive Polymer nano-bioComposites (CPC): Chitosan-carbon nanoparticle a good candidate to design polar vapour sensors. *Sens. Actuators B Chem.* **2009**, *138*, 138–147.

80. Chatterjee, S.; Castro, M.; Feller, J.F. An e-nose made of carbon nanotube based quantum resistive sensors for the detection of eighteen polar/nonpolar VOC biomarkers of lung cancer. *J. Mater. Chem. B* **2013**, *1*, 4563.

81. Joulazadeh, M.; Navarchian, A.H. Ammonia detection of one-dimensional nano-structured polypyrrole/metal oxide nanocomposites sensors. *Synth. Met.* **2015**, *210 (Part B)*, 404–411.